THE JOURNAL OF PHYSICAL CHEMISTRY B

Article

pubs.acs.org/JPCB

Interfacial Thermodynamics of Water and Six Other Liquid Solvents

Tod A. Pascal*,† and William A. Goddard, III*

Materials and Process Simulation Center, California Institute of Technology, Pasadena, California 91125, United States

Supporting Information

ABSTRACT: We examine the thermodynamics of the liquid−vapor interface by direct calculation of the surface entropy, enthalpy, and free energy from extensive molecular dynamics simulations using the two-phase thermodynamics (2PT) method. Results for water, acetonitrile, cyclohexane, dimethyl sulfoxide, hexanol, *N*-methyl acetamide, and toluene are presented. We validate our approach by predicting the interfacial surface tensions (IFT—excess surface free energy per unit area) in excellent agreement with the mechanical calculations using Kirkwood−Buff theory. Additionally, we evaluate the temperature dependence of the IFT of water as described by the TIP4P/2005, SPC/Ew, TIP3P, and mW classical water models. We find that the TIP4P/2005 and SPC/Ew water models do a reasonable job of describing the interfacial thermodynamics; however, the TIP3P and mW are quite poor. We find that the underprediction of the experimental IFT at 298 K by these water models results from understructured surface molecules whose binding energies are too weak. Finally, we performed depth profiles of the interfacial thermodynamics which revealed long tails that extend far into what would be considered bulk from standard Gibbs theory. In fact, we find a nonmonotonic interfacial free energy profile for water, a unique feature that could have important consequences for the absorption of ions and other small molecules.

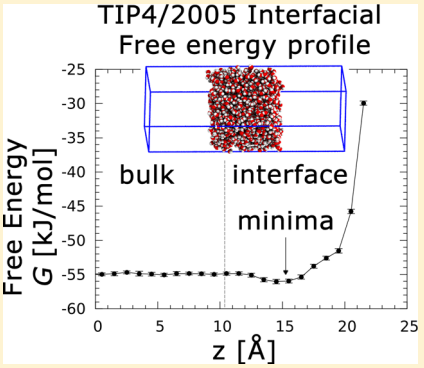

1. INTRODUCTION

Quantifying the interfacial properties of liquids is critical for understanding physical phenomena ranging from solvation of biomolecules to cloud formation,[1] and even industrial separations and oil recovery.[2] Yet for even the most basic air−water interface, questions about the orientation of interfacial water molecules,[3−7] the surface potential,[8−10] and the propensity and population of interfacial ions[11,12] are still subject to debate. We are interested in obtaining an atomic level understanding of the thermodynamics of water and other common liquids,[13−15] with the ultimate aim of quantifying the role of entropy in biomolecular and electrochemical processes.[16−19] To this end, we report here the thermodynamics at the liquid−vapor interface, with primary focus on the interfacial surface tension (IFT).

Consider an air−liquid interface at thermodynamic equilibrium. The IFT γ is defined as the free energy required to increase the surface area A by 1 unit, at constant temperature T, pressure P, and number of molecules N.:

$$\gamma = \left(\frac{\partial G}{\partial A}\right)_{N,T,P} = \left(\frac{G_{\text{surface}} - G_{\text{bulk}}}{\partial A}\right)_{N,T,P} \quad (1)$$

According to the Gibbs−Helmholtz relation ($G = A + PV$) and the Helmholtz expression of free energy ($A = U - TS$), we can rewrite eq 1 in terms of contributions from the surface enthalpy[20] (H) and entropy (S):

$$\gamma = \left(\frac{H_{\text{surface}} - H_{\text{bulk}} + TS_{\text{surface}} - TS_{\text{bulk}}}{\partial A}\right)_{N,T,P} = \left(\frac{\Delta h_{\text{ex}} - T\Delta s_{\text{ex}}}{\partial A}\right) \quad (2)$$

where h_{ex} and s_{ex} are the molar excess surface enthalpy and entropy, respectively.

Using standard molecular dynamics (MD) simulations, the surface enthalpy can be obtained simply as the potential energy difference between a bulk (three-dimensional (3D) periodic) and slab (2D periodic) geometry of the same system, corrected for any differential volume, heat capacity, and quantized vibrational effects. However, eq 2 is seldom, if ever, used to evaluate the IFT due to the enormous computational cost required to obtain the entropy using standard techniques such as thermodynamic integration (TI) or free energy perturbation theory (FEP). Rather, various indirect methods have been developed, including recent examples based on area sampling,[21−24] volume sampling,[25] and capillary waves.[26] However by far the most popular indirect method is based on the rigorous statistical mechanical formulism first proposed by Tolman[27] and later developed more fully by Kirkwood and Buff (KB):[28]

$$\gamma = \frac{1}{2}\int\left[p_{\perp}(z) - \frac{1}{2}\{p_{\parallel_a}(z) + p_{\parallel_b}(z)\}\right]dz \quad (3)$$

Received: November 4, 2013
Revised: May 12, 2014
Published: May 12, 2014

Table 1. Description of Liquid Systems Considered in This Study[a]

				ρ (g/cm^3) at 298 K[b]		slab simul param		
liquid	FF	no. of mol	⟨vol⟩ (Å^3)	calc (this work)	expt[c]	syst dimens	G-vector	K-space grid
water	SPC/Ew	1728	52068.5	0.992	0.998	36.9 × 36.9 × 136.9	0.291	30 × 30 × 160
	TIP3P	1728	48896.2	1.057	0.998	34.7 × 34.7 × 134.7	0.29	30 × 30 × 160
	TIP4P/ 2005	1728	52383.4	0.986	0.998	37.2 × 37.2 × 137.2	0.302	36 × 36 × 180
	mW	1728	51813.4	0.997	0.998	36.7 × 36.7 × 136.7		
acetonitrile	OPLS/ AA-L	512	48154.4	0.725	0.786	36.8 × 36.8 × 136.8	0.254	30 × 30 × 205
cyclohexane	OPLS/ AA-L	180	33327.8	0.755	0.779	32.2 × 32.2 × 132.2	0.22	15 × 15 × 125
hexanol	OPLS/ AA-L	160	33717.8	0.805	0.813	32.5 × 32.5 × 132.5	0.247	24 × 24 × 165
DMSO	OPLS/ AA-L	320	37675.9	1.102	1.100	33.6 × 33.6 × 133.6	0.244	24 × 24 × 160
NMA	OPLS/ AA-L	256	32437.2	0.958	0.957	32.0 × 32.0 × 132.0	0.253	25 × 25 × 185
toluene	OPLS/ AA-L	200	35723.3	0.857	0.866	33.1 × 33.1 × 133.1	0.225	18 × 18 × 120

[a]The force fields (FF) used are indicated. The average volume and density are taken from statistical averaging of the last 1 ns of a 2 ns NPT bulk simulation. [b]ρ = bulk density. [c]From *NIST Chemistry Webbook*.[84]

where $p_\perp$ is the component of the stress tensor perpendicular to the surface (z-axis in our coordinate system), while $p_{\parallel a}$ and $p_{\parallel b}$ are the parallel (x- and y-axis) components. The great idea behind this KB method is that, in the bulk liquid, the parallel and perpendicular stress components are equal and cancel, while, at or near the interface, $2p_\perp > p_\parallel$. Thus eq 3 allows the IFT to be obtained from MD simulations by a simple integration of the components of the pressure. Originally developed for treating simple Lennard-Jonesian systems, the KB method has since been applied successfully to calculate the IFT of a vast number of complex molecular systems, including surfactants at water−oil interfaces,[29] and to several studies of pure water, mostly described by classical force fields.[22,26,30−40]

While the KB method is in principle exact, it does not provide direct insights into how differential molecular motions (surface entropy) and nonbond interactions (surface enthalpy) inform interfacial stability, insights that are critical for unravelling several unsolved mysteries.[41] With this in mind, we describe here a scheme for predicting the IFT from direct estimation of the surface energies. Our approach is based on the two-phase thermodynamics method (2PT) of Lin et al.,[42,43] where the absolute thermodynamics of a system is obtained from the correlations in the atomic velocities. We show that, with a minor modification, the 2PT method, originally developed for obtaining the thermodynamics of bulk, condensed phase systems, is equally valid for estimating the thermodynamics of 2D slab geometries. Due to the intense interest in water, we focus most of our discussion on the air−water interface, as described by the popular rigid SPC/Ew[44] and TIP4P/2005[45] water models. We also demonstrate the generality of our approach by predicting the IFT and examining the interfacial thermodynamics of six other common, organic solvents.

The remainder of this work is organized as follows. Section 2 presents a brief overview of the simulation methodology and 2PT method, and in section 3 we present and discuss our results, which are summarized in section 4.

2. THEORETICAL BACKGROUND AND COMPUTATIONAL METHODS

2.a. Two-Phase Thermodynamics Method of Estimating the Thermodynamics of Condensed Phase Systems. The details of the 2PT method have been presented elsewhere,[42,43] but we include a brief summary here. The 2PT method belongs to a broad class of approaches for obtaining the absolute thermodynamics of a system by integrating the density of states (DoS) function (also known as the spectral velocity or the power spectrum) with the quantum harmonic oscillator weighting function:[46]

$$q^{Q}_{HO}(\nu) = \frac{\exp(-\beta h\nu/2)}{1 - \exp(-\beta h\nu/2)} \tag{4}$$

The only difficulty with using eq 4 is that it produces a singularity at DoS(0); i.e., the DoS evaluated at $\nu = 0$ frequency. In solids, DoS(0) = 0, and the above approach is valid. However since DoS(0) is proportional to the self-diffusion constant,[47] which is always greater than zero for a liquid, this approach cannot be applied straightforwardly. Therefore, the unique feature of the 2PT method is to partition the total DoS into two components:

$$\mathrm{DoS}^{\mathrm{total}} = f \times \mathrm{DoS}^{\mathrm{gas}} + (1 - f)\mathrm{DoS}^{\mathrm{solid}} \tag{5}$$

where (1) $\mathrm{DoS}^{\mathrm{gas}}$ is a gas-like component which satisfies the condition that $\mathrm{DoS}(0) = \mathrm{DoS}^{\mathrm{gas}}(0)$ and whose thermodynamics is accurately obtained from the Carhanan−Starling equation of state for a warm dense fluid[48] or, more recently, from a memory function[49] and (2) $\mathrm{DoS}^{\mathrm{solid}}$ is a solid-like component with $\mathrm{DoS}^{\mathrm{solid}}(0) = 0$, thereby circumventing the singularity in eq 4.

This idea of describing water as a superposition of a gas and solid phase can be traced back to an original proposition of Eyring and Ree.[50] All that remains is to obtain f, the partition constant, which is expressed as the ratio of the self-diffusion constant of the system (or of the part of the system of interest) to that of a gas of the hard spheres, whose diffusion constant at the same temperature and density is obtained from Chapman−Enskog theory.[46]

One obvious advantage of the DoS-based approaches, such as 2PT, is the inherent efficiency due to the use of short MD trajectories. Indeed, previous studies have shown the 2PT method accurate in predicting the entropy of comparable accuracy to much more computationally demanding TI and FEP calculations.[13,51−53] Additionally, a unique feature of the 2PT method is that the absolute thermodynamics of arbitrary systems containing solids, liquids, and/or gases can be obtained from a single, equilibrated MD trajectory, without the need to either define a "reaction coordinate" (TI) or introduce additional perturbations into the system (FEP). To this end, several studies[54−60] have utilized the 2PT method to elucidate the thermodynamics of complex biological and inorganic systems. A third very important advantage is that all of the properties are ultimately sums over atomic properties, which means that we can examine the thermodynamics of individual molecules in a system.

dx.doi.org/10.1021/jp410861h | J. Phys. Chem. B 2014, 118, 5943−5956

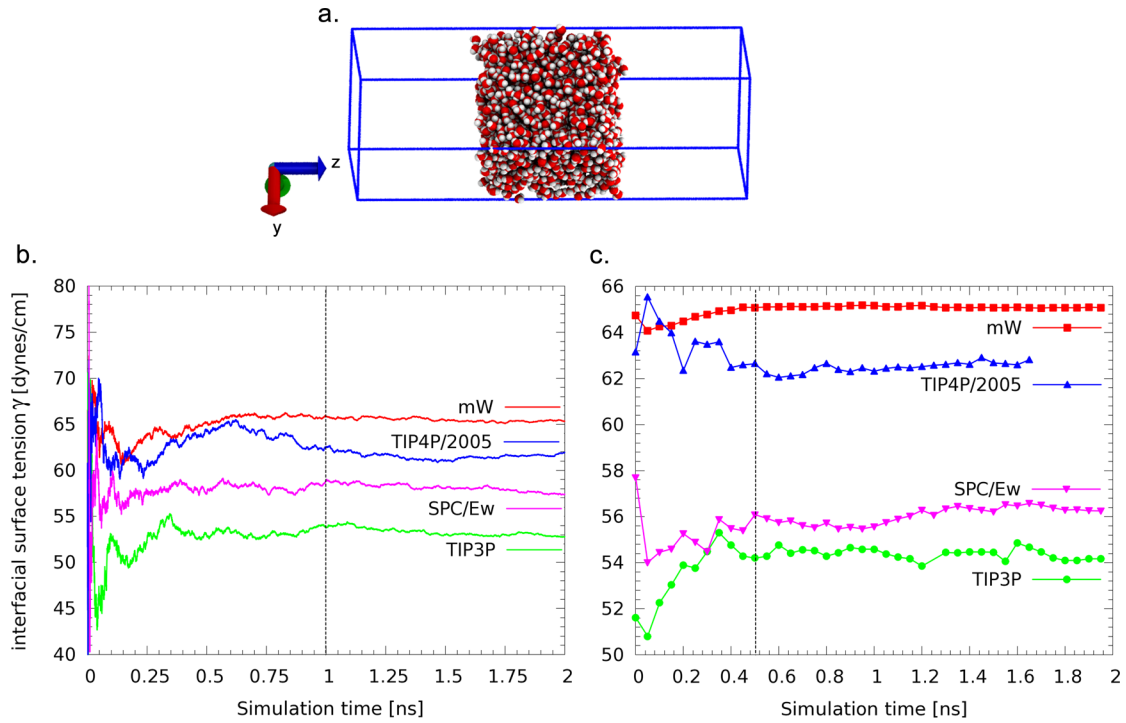

Figure 1. (a) Snapshot of the air−water simulation cell showing 1728 equilibrated TIP4P/2005 water molecules. The dimension of the cell are $L_x = L_y =$ 3.7 nm, L_z = 13.7 nm. There is 10 nm of vacuum in the z direction. Note that the surface is not flat; it fluctuates significantly due to capillary effects. (b) Interfacial surface tension (IFT) calculated using Kirkwood−Buff theory of water described by the mW (red line), TIP4P/2005 (blue line), SPC/Ew (pink line), and TIP3P (green line) as a function of time. The vertical dashed line at 1 ns indicates the point of convergence. (c) IFT of water as calculated using the 2PT method as a function of time. The color schemes for the various water models are the same as before. The convergence point is ∼0.5 ns.

2.b. Extending the 2PT Method for Systems with Open Boundaries. The f factor in eq 5 is obtained self-consistently during the MD simulation from the average density of the system, which is trivially obtained from the cell volume in a periodic, bulk simulation. However, slab geometries, such as the liquid−vapor interface, have open boundaries, so we define an effective volume by first fitting the density profile ρ to a hyperbolic function:

$$\rho_{\pm}(z) = a\left[1 \pm \tanh\left(-\frac{z - z_G}{\delta}\right)\right] \tag{6}$$

for the top (+) and bottom (−) surfaces, where a is a parameter related to half the bulk density, z_G is the location of the "Gibbs dividing surface", and δ is a parameter related to the interfacial thickness. Integration of eq 6 then produces the effective slab volume (V_{slab}):

$$V_{slab} = L_{xy}\int^{z/2} \rho_{\pm}(z)\,dz = L_{xy}a\left(1 \mp \delta \log\left(\cosh\left(-\frac{z - z_G}{\delta}\right)\right)\right) \tag{7}$$

2.c. Molecular Dynamics Simulation Methodology. We considered the interfacial thermodynamics of water, as described by the SPC/Ew,[44] TIP3P,[61] TIP4P/2005,[45] and mW[62] water models, as well as acetonitrile, cyclohexane, hexanol, dimethyl sulfoxide (DMSO), *N*-methyl acetamide (NMA), and toluene, all described with the OPLS AA/L[63,64] force-field field (Table 1). All simulations were performed using the LAMMPS[65] MD simulation engine. Bonds containing hydrogens and the H−O−H angles of the water molecules were constrained using the SHAKE[66] algorithm with a tolerance of 10^{-5}.

For each liquid, we performed a bulk simulation starting with a structure packed to minimize the interaction energy by applying the continuous configurational Boltzmann biased (CCBB) Monte Carlo (MC) method.[67,68] We then equilibrated the liquid using our standard procedure:[14] after an initial conjugate gradient energy minimization to a root mean square (RMS) force of 10^{-5} kcal/(mol/Å), we heated the system from 0 K to the desired temperature over 100 ps in the constant volume, constant temperature (canonical or *NVT*) ensemble with a Langevin thermostat. The temperature damping constant was 0.1 ps, and the simulation time step was 1.0 fs. Long-range Coulombic interactions were calculated using the particle−particle particle−mesh (PPPM) method[69] (with a precision of 10^{-5} kcal/mol), while the van der Waals (vdW) interactions were computed with a cubic spline (inner cutoff of 11 Å and an outer cutoff of 12 Å). We used the spline to guarantee that the energies and forces go smoothly to zero at the outer cutoff, thereby preventing discontinuities. We tested the effect of the cutoff parameters by computing the potential energy of the box of acetonitrile molecules with cutoffs ranging from 8 to 20 Å and found convergence to the limiting value of −37.9 kJ/(mol/molecule) at 10 Å (Supporting Information Figure S1).

After initial equilibration, we performed a 1 ns simulation within the constant pressure (1 bar), constant temperature (isothermal-isobaric, or *NPT*) ensemble. The temperature damping constant was 0.1 ps while the pressure piston damping constant was 2.0 ps. The equations of motion used were those of Shinoda et al.,[70] which combine the hydrostatic equations of Martyna et al.[71] with the strain energy proposed by Parrinello

dx.doi.org/10.1021/jp410861h | J. Phys. Chem. B 2014, 118, 5943−5956

and Rahman.[72] The time integration schemes closely follow the time-reversible measure-preserving Verlet integrators derived by Tuckerman et al.[73] Production dynamics were then run for a further 2.5 ns in the *NPT* ensemble. We saved a restart file (simulation cell parameters, thermostat and barostat parameters, and atomic coordinates and velocities) every 100 ps.

Starting from the equilibrated bulk coordinates and velocities, we then performed a slab calculation for each liquid. We first inflated the *z*-dimension of the simulation cell by 10 nm and centered the liquid slab within the cell, thus allowing 5 ns of vacuum at each surface (Figure 1a). The top and bottom of the simulation box were bounded by a purely repulsive wall. After initial heating, we performed a 2D-*NVT* simulation for 4 ns. In all cases, the slab was found to be stable over the entire MD simulation; significant evaporation was only observed for liquid water near the boiling point. All simulation parameters were the same as the bulk simulations, and application of the 2D PPPM method resulted in **G**-vectors and *K*-space grids tabulated in Table 1. In order to remove spurious interactions between the two surfaces, we employed the 2D slab corrections of Yeh and Berkowitz[74] with a further 2.0 *z* factor. During the last 2 ns of dynamics, we saved a restart file every 100 ps.

2.d. Calculation of the Interfacial Surface Tension Using the 2PT method. For each of the 3D bulk and 2D slab restart files, we ran an additional 20 ps *NVT* simulation, saving the atomic velocities and coordinates every 4 fs. The absolute entropy, quantum-corrected enthalpy, and Helmholtz free energy were obtained by post-trajectory analysis using an in-house code that implements the 2PT method. The IFT was calculated according to eqn. (1) as:

$$\gamma^{2PT} = c\frac{SE}{SA} = c\frac{G_{slab} - G_{bulk}}{SA} \quad (8)$$

where $c = 166.03$ is the conversion factor to go from kJ/(mol/A^2) to dynes per centimeter, and SE is the surface energy, calculated as the free energy difference between the N_{mol} bulk and slab waters. The surface area, SA, was taken as the 2 times the cell $L_x \times L_y$ area (the factor of 2 accounting for both surfaces). We obtained a depth profile of the thermodynamics as a function of the distance from the surface by discretizing the average *z* component of the center of mass of each molecule (over the 20 ps of MD) on a cubic grid. The grid length was chosen to be the minimum required so that the density at the center of the slab equaled the bulk density. We found that grid lengths of ∼2 Å generally led to good results. The thermodynamics of the molecules at each grid point were then grouped and averaged.

2.e. Interfacial Surface Tension Calculations from KB Method. The equilibrated atomic coordinates and velocities of each slab were used as input for an additional 10 ns *NVT* simulation. Snapshots of the system (coordinates, velocities, and the six-component pressure tensor) were saved every 100 fs, and the IFT was calculated from eq 3 by integrating the cumulative pressure tensor in 0.1 Å slabs along the *z*-axis. Statistical averaging and uncertainties were estimated from partitioning the 10 ns simulation into five blocks (each 2 ns long).

3. RESULTS AND DISCUSSION

3.a. Comparison of KB and 2PT IFT at Room Temperature. Table 2 compares the IFT calculated using the 2PT and KB methods. We find very good agreement between the two approaches for all 10 liquids, with a 98% correlation coefficient (Supporting Information Figure S2), a mean absolute error of 1.9 dyn/cm, and an unsigned error of 2.1 dyn/cm (∼5%). Overall,

Table 2. Comparison of Experimental and Calculated Interfacial Surface Tension (IFT, dyn/cm) of the Liquids at 298 K[a]

		γ^{KB}		γ^{2PT}	
	γ^{expt}[b]	av	std dev	av	std dev
TIP4P/2005	71.9	63.5	0.5	64.4	0.7
mW	71.9	65.3	0.4	66.9	0.6
SPC/Ew	71.9	57.4	0.4	55.8	0.7
TIP3P	71.9	52.8	0.4	52.6	1.0
acetonitrile	28.7	9.6	0.8	10.2	0.7
cyclohexane	24.2	17.0	0.7	14.2	0.4
dmso	42.9	50.1	0.7	44.6	1.3
hexanol	23.8	18.7	0.8	15.1	2.1
nma	31.0	39.0	0.9	38.1	2.5
toluene	27.7	23.9	0.5	20.2	0.4

[a]The calculated IFT using the Kirkwood−Buff (KB) and two phase thermodynamics (2PT) methods are presented. [b]Experimental values from ref 82.

the 2PT method underestimates the IFT by ∼1.5 dyn/cm (∼3%) compared to KB theory. The largest discrepancy occurred for DMSO (−5.5 dyn/cm or ∼11%) and toluene (−3.7 dyn/cm or ∼15%). The agreement between the two approaches improves significantly if we only consider the four water models: the 2PT method is found to be within 0.2 dyn/cm of KB theory (∼0.3%).

One possible source of error is the reported underestimation of the entropy by the 2PT method,[43,52] although this effect should be mitigated by cancellation of errors in the bulk and slab entropies. More likely, our assumption of a planar interface, where the surface area is taken to be the $L_x \times L_y$ cell dimensions, introduces some errors. The liquid−vapor interface is distinctly not planar, but rather is characterized by significant density fluctuations[75−79] at room temperature. These fluctuations would increase the surface area and so decrease the surface tension. However, this does not explain the underestimation of the IFT in the case of the larger organic liquids. For these systems, it is possible that the calculated thermodynamics are not converged on the 20 ps time scale used to evaluate the thermodynamics. The 2PT method relies on short trajectories to evaluate the thermodynamics, and one may reasonably wonder if a 20 ps trajectory is sufficient to properly sample the soft (lower frequency) modes of these more complex liquids. As a test case to check the effect of trajectory sampling length on the calculated IFT, we considered hexanol, where the IFT predicted by our 2PT approach is 15.1 ± 2.1 dyn/cm using a 20 ps trajectory window, about 23% less than the KB value of 18.7 ± 0.8 dyn/cm. By increasing the trajectory sampling window length to 25, 50, and 100 ps, we find that the 2PT-IFT increases to 15.9, 16.7, and 17.1 dyn/cm, respectively. In fact, using 40 ps instead of 20 ps trajectories reduces the average 2PT-IFT error from 5% to 2%, confirming our hypothesis.

3.b. Comparison to Other Published Results for Water at 298 K. Even for the same water model, the KB-IFT values reported in the literature show significant variation depending on the simulation methodology (cutoffs, treatment of long-range electrostatics, and so on), making it difficult to place our results in the proper context. For example, previous studies[26,80] have demonstrated that the calculated IFT is strongly dependent on the treatment of long-range electrostatics.[24,75] Consistent with these studies, we find that our KB-IFT results using the SPC/Ew water model and the PPPM scheme is in very good agreement with the analogous particle mesh Ewald results of Vega and de

dx.doi.org/10.1021/jp410861h | J. Phys. Chem. B 2014, 118, 5943−5956

Table 3. Bulk, Absolute Molar Free Energy ($G°$, kJ/mol), Enthalpy ($H°$, kJ/mol), and Entropy ($S°$, J/(mol/K)), Specific (Excess) Enthalpy (H_{ex}, kJ/km^2) and Entropy (S_{ex}, J/(K/km^2)), and the Heat of Vaporization ΔH_{vap} (kJ/mol) of Water and Various Common Solvents at 298 K As Calculated by the 2PT Method Compared to Experiment

	bulk energy							specific surface energy			
	$G°_{liq}$		$H°_{liq}$		$S°_{liq}$			H_{ex} (kJ/km^2)		S_{ex} [J/(K/km^2)]	
	av	std dev	av	std dev	av	std dev	ΔH_{vap}	av	std dev	av	std dev
TIP4P/2005	−54.9	0.1	−37.5	0.1	58.4	0.2	45.6	107.5	2.9	144.7	2.9
mW	−53.4	0.1	−35.9	0.1	58.7	0.1	44.6	87.3	0.7	51.4	1.4
SPC/Ew	−54.7	0.1	−36.5	0.1	61	0.2	45	103.4	3.1	158.3	4.4
TIP3P	−54.1	0.1	−33.1	0.1	72.1	0.2	42.6	104.5	3.5	174.2	4.3
expt	−54.9		−34.1[a]		69.9[b]		44	117.8		154.1	
acetonitrile	−58.3	0.2	−16.3	0.3	140.7	1.3	35.7	72.7	2.4	209.6	3.1
expt[c]	−65.8	0.3	−21	0.3	149.6	0.1	32.9	66		126	
cyclohexane	52.2	0.3	108.9	0.5	190.3	1.5	29.2	79	0.5	217.3	5.1
expt	−76.1	0.2	−15.5	0.4	203.5	1.3	33	59		116.7	
DMSO	−17.4	0.2	31	0.3	162.5	1.1	48.8	104.3	1.7	200	3.8
-Expt.					188.8	0.3	52.9	76.9		114.4	
hexanol	7.6	0.6	77	0.9	232.9	2.3	52.6	61.9	1.6	157	4.2
expt	−55.3	1.7	31.8	2.5	287.4	1.4	61.6	47.6		80	
NMA	−33.5	0.3	−1.2	0.3	176.2	1.3	55.2	96.1	0.8	194.5	1.6
expt			38.5	5.8			59.8	68		124.2	
toluene	11.3	0.3	69.8	0.5	196.3	2	39.6	85.9	0.9	220.6	6.9
expt	−45.7	0.5	20	0.3	220.5	0.9	38	63.3		118.9	

[a] $H°$ is obtained from ΔH in ref 85 by $H° = \Delta H - (3RT + PV)$ which is the work to bring a single molecule in the gas phase into the liquid. [b] Reference 84. [c] Expermental $G°$ and $S°$ from NIST/TRC Web thermotables,[96] $H°$ is obtained from ΔH_{vap} by $H° = \Delta H_{vap} - (H_{IG} + PV)$, where ΔH_{vap} is the heat of vaporization and H_{IG} is enthalpy of an ideal gas, obtained from the integral of the specific heat capacity.

Miguel[22] and Chen and Smith,[39] but is ∼6% greater than the Ewald results of Ismail et al.[26] Other studies have suggested that the calculated IFT should be augmented by tail corrections,[26] presumably to account for the dispersion contributions to the pressure beyond the van der Waals cutoff. In order to investigate this effect, we calculated the IFT while varying the vdW cutoffs of the TIP4P/2005 water model from 0.8 to 2.0 nm (Supporting Information Figure S3). We find that, for both approaches, the IFT increases with increasing cutoff and asymptotically converge to 66.9 and 67.3 dyn/cm for the KB and 2PT methods, respectively. This translates to an effective tail correction of 2.3 and 2.9 dyn/cm, respectively, somewhat less than the 4.1 dyn/cm tail correction suggested by Vega and de Miguel.[22] A 2 nm van der Waals cutoff would increase our simulation time by ∼50%, however, so we consider the 1.2 nm cutoff a good compromise between speed and accuracy.

3.c. Efficiency of the 2PT/KB Method for Evaluating Surface Tension of Water. For a homogeneous liquid, whose potential energy surface might be characterized by many low-lying, quasi-degenerate local minima, it is necessary to sample many short trajectories in order to fully characterize the system thermodynamics using the 2PT method. This leads naturally to the following questions: (1) how many independent trajectories are necessary to obtain converged IFTs and (2) how does the convergence time compare to the KB method? As shown in Figure 1b, the KB-IFT of water takes at least 1 ns to converge, or in the case of the TIP4P/2005 water model, as long as 1.5 ns. This calls into question reported results using only 300 ps trajectories.[80] We find that the KB-IFT of the coarse grained, charge-less mW water model converges faster (∼0.6 ns) than any of the atomistic, point charge water models, possibly indicating that Friedel-like oscillations[81] in the long-range electrostatics are responsible for the longer convergence times.

In contrast, we find that the 2PT-IFT of water converges within ∼0.5 ns, making it 2−3 times faster than KB. The convergence time for the pressure is expected to be longer than the thermodynamics (entropy) since the pressure is particularly sensitive to fluctuations at the interface and hence to capillary waves. On the other hand, the 2PT entropy is based on the DoS, which converges on the time scale of <100 ps due to frequent molecular collisions. The 2PT convergence time is consistent with previous results on bulk liquids,[14] suggesting that the thermodynamics, and particularly the entropy, of water in a slab geometry converges on a time scale similar to the bulk.

3.d. Comparison to Experimental IFT of Water. Using a vdW cutoff of 1.2 nm, we find that all four water models underestimate the experimental IFT of water, 71.9 dyn/cm[82] (Table 2). The coarse grained mW water model (65.3 ± 0.4 dyn/cm for KB and 66.9 ± 0.6 dyn/cm for 2PT) shows the closest agreement to experiment, consistent with the findings of another study,[83] while the TIP3P water model (underestimated by ∼27%) shows the worst agreement. The popular SPC/Ew and TIP4P/2005 water models are found to underestimate the IFT by ∼20% and ∼10%, respectively. A natural question is, what is the thermodynamic basis for the underestimation of the experimental IFT by these popular water models? An advantage of the 2PT-based approach is that we can attempt to answer this question by considering separately the enthalpic and entropic contributions to the IFT and indeed the contributions to the waters in various layers. According to the definition of the IFT in eq 1, we know that any errors in the calculated IFT must arise from either an incorrect thermodynamic description of the bulk liquid, the interface, or both. We first consider the bulk liquid.

The experimental molar entropy, $S°$, of water under standard conditions (298 K and 1 atm) is 69.9 J/(mol/K),[84] the standard molar enthalpy, $H°$, is −34.1 kJ/mol, and the standard molar free energy, $G°$, is −54.9 kJ/mol. Experimentally, the molar entropy can be obtained from an integration of the specific heat capacity, while the enthalpy can be obtained by subtracting the enthalpy of

dx.doi.org/10.1021/jp410861h | J. Phys. Chem. B 2014, 118, 5943−5956

an ideal gas from the heat of vaporization, ΔH_{vap} (the experimental value at 298 K is −44 kJ/mol[85]):

$$H^\circ = \Delta H_{vap} - (3RT + PV) \quad (9)$$

Our results indicate that all four water models predict G° to within 0.7 kJ/mol, or ∼1% (Table 3), with the TIP4P/2005 (−54.9 ± 0.1 kJ/mol) and SPC/Ew (−54.7 ± 0.1 kJ/mol) being especially accurate. However, the accuracy in predicting the bulk liquid free energy results from a cancellation of errors between the underpredicted entropy and the overpredicted enthalpy.[13] Further, even though the enthalpy is overpredicted, ΔH_{vap} is found to be in excellent agreement with experiment (Table 3), which is not surprising given that ΔH_{vap} is commonly used as a fitting parameter when developing the water model. Our results clearly show, however, that fitting to ΔH_{vap} is not sufficient and should not be taken as evidence that the water model concurrently describes the bulk and vapor phase enthalpies correctly.

The accuracy in predicting the bulk free energies thus suggests that the underprediction of the water IFT arises from an incorrect thermodynamics description of the interface. When investigating interfacial thermodynamics, we find it more convenient to consider the specific (excess) enthalpy, ΔH_{ex}, and entropy, ΔS_{ex}:

$$\Delta H_{ex} = A\Delta h_{ex}, \quad \Delta S_{ex} = A\Delta s_{ex} \quad (10)$$

where h_{ex} and s_{ex} are molar quantities defined in eq 2 and A is the surface area. Physically, the specific surface enthalpy is a measure of the two-body nonbonded interactions at the interface: an underestimation indicates that surface interactions are too repulsive; i.e., the interactions between the surface molecules are not strong enough. Alternatively, the specific surface entropy is a measure of the many-body correlated motions at the interface: an underestimation indicates overstructuring of the surface molecules. The reason for considering the excess surface energies is that they can be directly compared to experimental measurements. If we consider small changes in the temperature, the surface enthalpy is constant and

$$\left(\frac{\partial \gamma}{\partial T}\right)_P = \left(\frac{\partial H_{ex}}{\partial T} - \frac{\partial}{\partial T} T\Delta S_{ex}\right)_P = -\Delta S_{ex} \quad (11)$$

Using the surface tension results from the International Association for the Properties of Water and Steam (IAPWS) tables,[86] we calculate ΔS_{ex} = 154.1 J/(K/m^2) at 298 K, which, when considering the IFT at 298 K of 71.9 kJ/m^2 (dyn/cm), means that ΔH_{ex} = 117.8 kJ/m^2.

As shown in Table 3, all four water models underestimate the excess surface enthalpy compared to experiment; however, there are significant variations in the excess surface entropy. First, we find that the mW water model significantly underestimates both the excess surface enthalpy (−26%) and the excess surface entropy (−67%). Thus the good agreement to the experimental excess surface free energy (IFT) results from a large cancellation of errors. On the other hand, the TIP3P water model underestimates the excess surface enthalpy (−12%) but overestimates the excess surface entropy (+13%), resulting in an IFT that is significantly too low. The TIP4P/2005 water model greatly improves on the performance of the TIP3P water model: the errors in the excess surface enthalpy (−8%) and entropy (−6%) both decrease and perhaps more importantly, compensate each other. The net result is that the IFT is in very good agreement with experiment. Finally, the excess surface enthalpy of the SPC/Ew water model is in excellent agreement with experiments (overestimated by ∼2.3%, within the error bars of our calculations), which means that the underestimation of the experimental IFT is almost purely due to a 13% underestimation of the excess surface enthalpy.

In addition to establishing the thermodynamic basis for the underestimation of the experimental IFT, our results suggest new metrics to consider when selecting a water model suitable for describing interfacial properties. First, it is clear that the TIP3P water model is particularly poor at describing the air−water interface: the interfacial water molecules are both not cohesive enough (the excess surface enthalpy is too low) and overstructured. Introduction of an off-center site for the oxygen charge and optimization of the partial atomic charge and oxygen van der Waals terms, as was done for the TIP4P/2005 water model, greatly improves the description. However, our results indicate that the use of an off-centered charge site may not be essential, since the SPC/Ew, a three-site water model, is particularly good at describing the surface entropy. More sophisticated water models introduce additional terms, such as atomic polarization, which have been shown to improve the agreement to the experimental IFT.[87] This could indicate an improvement in describing the interactions of the surface molecules. However, these corrections would need to be evaluated within the context of the surface enthalpy and entropy to ensure that the observed improvements in the surface tension is not the result of cancellation of errors.

3.e. Comparison to the Experimental IFT of Other Liquids at 298 K. In Table 2, we compare the IFTs of the six other organic liquids to experiment. These liquids can be grouped into three main groups depending on their dielectric constants, miscibility in water, and ability to participate in hydrogen bonding:[14] (1) polar protic liquids with high dielectric constants that form hydrogen bonds with water, N-methyl acetamide (NMA) and hexanol; (2) polar aprotic liquids with medium dielectric constants that do not form hydrogen bonds with water, acetonitrile (H3C-C≡N) and dimethyl sulfoxide (DMSO); and (3) nonpolar liquids with low dielectric constant that are insoluble in water, cyclohexane and toluene.

We find that the OPLS/AA force field predicts IFTs in reasonable agreement with experiment, with an average error of ∼6 dyn/cm, except for acetonitrile, where the experimental IFT of 28.7 dyn/cm is significantly underestimated by both KB (9.6 ± 0.8 dyn/cm) and 2PT (10.2 ± 0.7 dyn/cm) (Supporting Information Figure S4). Another study[88] has also shown that the OPLS/AA force field underestimates the IFT of this liquid. Further, and in contrast to our results for water, thermodynamic analysis indicates that the errors in the calculated IFT results from overestimation of the excess surface entropy (Table 3). Indeed, in the case of acetonitrile, the experimental bulk entropy, enthalpy, and heat of vaporization are found to be well reproduced by the OPLS/AA force field, and the calculated excess surface enthalpy of 72.7 kJ/m^2 is in reasonable agreement with the experimental value of 66.0 kJ/m^2. However, the calculated excess surface entropy of 209.6 kJ/m^2 is more than 66% greater than experiment, indicative of surface molecules that are understructured (too disordered).

Another interesting case is toluene, where the calculated 2PT-IFT of 20.2 ± 0.4 dyn/cm (23.9 ± 0.5 dyn/cm from KB theory) is in reasonable agreement with the experimental value of 27.7 dyn/cm. However, this agreement obscures the fact that the excess surface entropy is overestimated by 101.7 kJ/m^2 (∼85%),

dx.doi.org/10.1021/jp410861h | J. Phys. Chem. B 2014, 118, 5943−5956

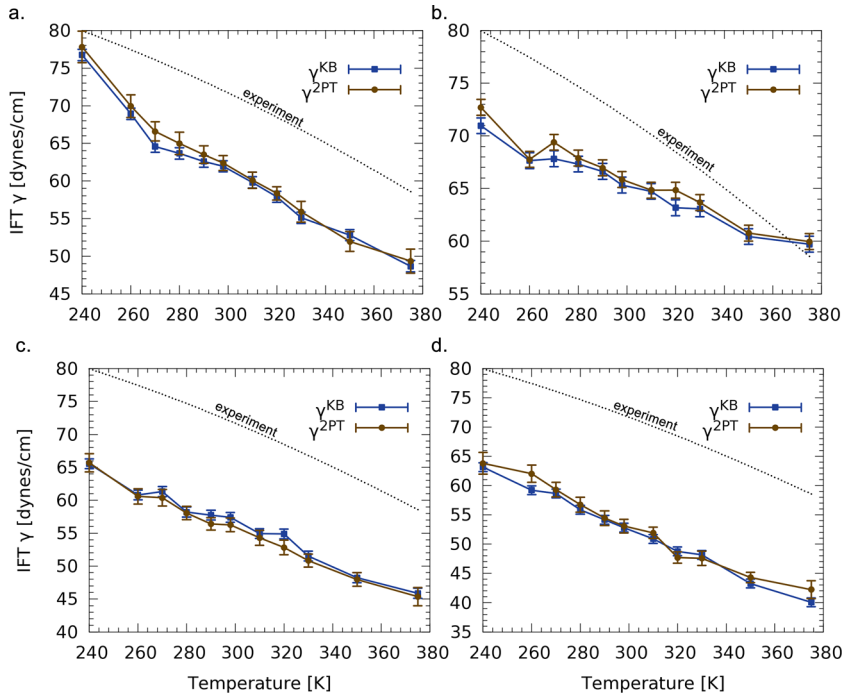

Figure 2. Surface tension of water, calculated using the Kirkwood–Buff (blue squares) and 2PT (brown circles) methods as a function of temperature from 240 to 375 K. Solid lines of the same color as the symbols are included to guide the eyes. The statistical uncertainty (standard deviation 1σ) is indicated by vertical error bars. The experimental data (refs 85 and 87; black dashed line) are included for comparison. Results for the (a) TIP4/2005, (b) mW, (c) SPC/Ew, and (d) TIP3P water models are shown.

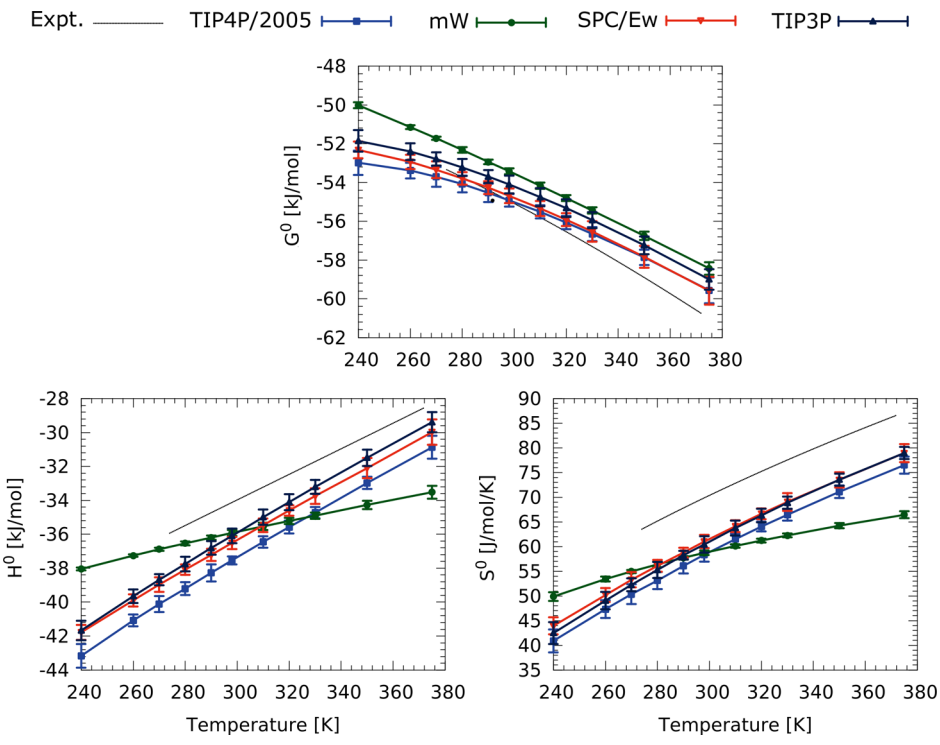

Figure 3. Thermodynamics [(a) $G°$, (b) $H°$; and (c) $S°$] of bulk water with temperature as described by the TIP4P/2005 (blue squares), mW (green circles), SPC/Ew (red down-triangles), and TIP3P (blue up-triangle) water models. Experimental values from 273 to 375 K obtained by subtracting off the respective ideal gas phase values at the liquid density from the experimental enthalpies and entropies of vaporization (data taken from ref 45).

while the excess surface enthalpy is also overestimated by 22.6 kJ/m^2 (~36%).

Overall, we find that the excess surface entropy of all six liquids is overestimated by ~77% on average, suggesting a fundamental limitation of the OPLS/AA for describing the vapor–liquid interface. The lack of polarization and/or charge rearrangement inherent in this fixed charge force field appears to affect both the cohesiveness of the surface molecules and their relative intermolecular motions, resulting in surface molecules that do not attract each other enough and are too disordered.

dx.doi.org/10.1021/jp410861h | J. Phys. Chem. B 2014, 118, 5943–5956

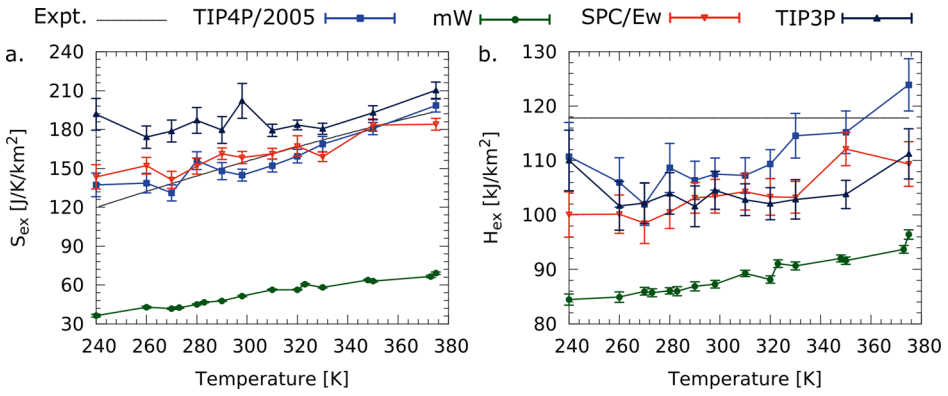

Figure 4. Specific surface thermodynamics (excess thermodynamics per unit area) of water from 240 to 375 K. The experimental results (black lines) are compared to calculated results using the TIP4/2005 (blue squares), mW (green circles), SPC/Ew (red down triangle), and TIP3P (dark blue up triangle) water models. (a) Specific surface entropy, S_{ex} [J/(K/km^2)]. The experimental values are obtained from the slope of the surface tension, assuming that the specific surface enthalpy is temperature independent. (b) Specific surface enthalpy, H_{ex} (kJ/km^2).

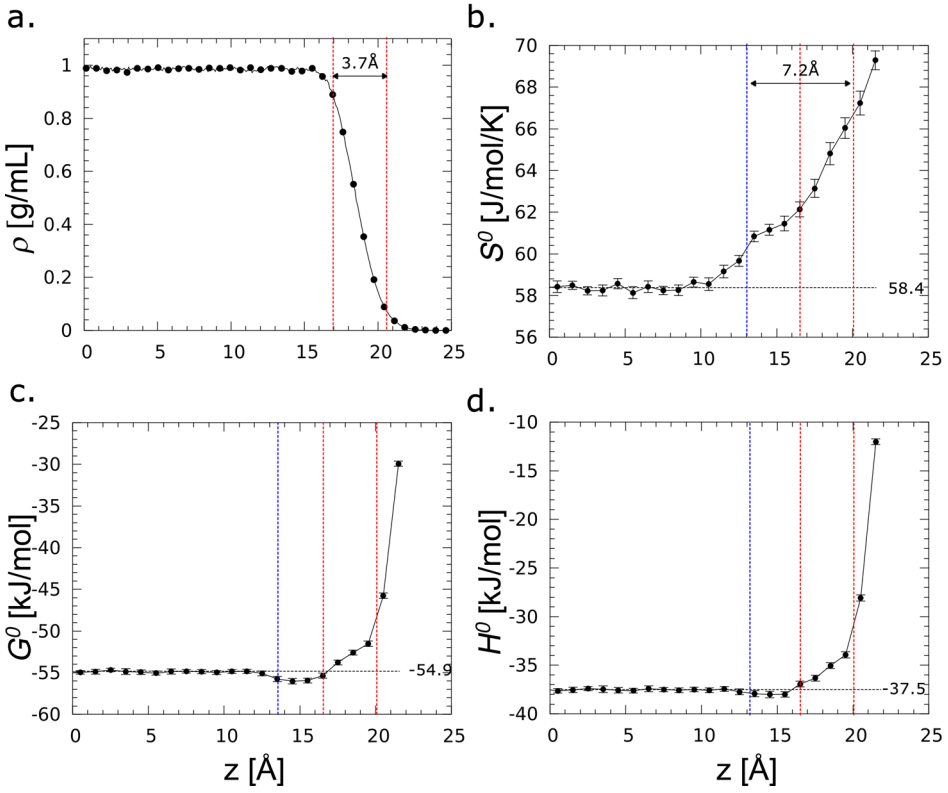

Figure 5. (a) Density profile, ρ, for a slab of 1728 TIP4P/2005 water molecules at 298 K. The density defined [90,10] interfacial thickness (3.7 Å) obtained from fitting a hyperbolic function in eq 6 is indicated by the dashed red lines. (b) $S°$ profile calculated using the 2PT method. The red dashed vertical lines represent the interfacial thickness in a. The vertical blue line denotes the distance of 90% of the bulk free energy. The free energy defined interfacial thickness (7.2 Å) is indicated as the difference between the vertical solid blue and red lines. (c) $G°$ profile calculated using the 2PT method. The bulk free energy (−54.9 kJ/mol) is indicated by the black horizontal dashed line. The color schemes of the dashed lines are the same as those in b. (d) $H°$ profile calculated using the 2PT method.

3.f. Temperature Dependence of the Surface Tension of Water. The importance of accurately predicting the excess surface entropy at 298 K extends beyond properly describing the interfacial structure at the standard temperature. In fact, the excess surface entropy at 298 K is a measure of accuracy in predicting the temperature dependence of the surface tension. Consider, for example, the SPC/Ew water model where we show the calculated IFT as a function of temperature (from 240 to 375 K) in Figure 2c. Although the absolute IFT is consistently underestimated, we find excellent agreement with experiments in the slope of the IFT. Further analysis reveals that the bulk free energy (Figure 3a) and excess surface entropy (Figure 4a) are in excellent agreement with experiment, while the bulk enthalpy (Figure 3b) and entropy (Figure 3c) are both underestimated (and compensate each other) over the temperature range. Additionally, and consistent with expectations, we find that the excess surface enthalpy is nearly constant over the temperature range (Figure 4b). Similar results were found for the TIP4P/2005 water model, which also predicts the excess surface tension at 298 K in good agreement with experiment. On the other hand,

dx.doi.org/10.1021/jp410861h | J. Phys. Chem. B 2014, 118, 5943−5956

although the mW water model predicts the IFT in excellent agreement with experiment at room temperature, it shows particularly poor agreement at other temperatures, as expected from the poor prediction of the excess surface entropy at 298 K.

In order to better quantify the temperature dependence of the surface tension of water, we note that, experimentally, the IFT from 273 to 373 K shows a slight quadratic decrease in the surface tension of water with temperature:[86,89−93]

$$\gamma_t = A - Bt - Ct^2 \tag{12}$$

where A = 74.86−77.27 dyn/cm, B = 0.0913−1.595 dyn/(cm/K), and $C = (0.1072-0.3986) \times 10^{-3}$ dyn/(cm/T^2). Applying eq 12 to our results for the SPC/Ew water model leads to A = 100.37 dyn/cm, B = 0.152 dyn/(cm/K), and $C = 0.136 \times 10^{-3}$ dyn/(cm/T^2) using the KB method and A = 105.87 dyn/cm, B = 0.156 dyn/(cm/K), and $C = 0.2660 \times 10^{-3}$ dyn/(cm/T^2) using the 2PT method. Alternatively, the temperature dependence of the surface tension of water can be predicted from the van der Waals equation for surface tension of liquids:

$$\gamma_T = A\tau^n \tag{13}$$

where $\tau = 1 - T/T_c$, A is an energy constant, and n is 1.25 for most liquids. Vargaftik et al. fitted the water surface tension values from the IAPWS tables[86] and came up with a modified expression that better fit the data:

$$\gamma_T = A\tau^{\mu}(1 + b\tau) \tag{14}$$

where A = 235.8 dyn/cm, T_c = 647.1 K, μ = 1.256, and b = −0.625. An intriguing aspect of eq 14 is that it predicts an inflection point (T_i) in the surface tension of water:

$$\frac{d^2\gamma}{d\tau^2} = \mu A\tau^{\mu-2}[b(\mu+1)\tau + (\mu-1)] \Rightarrow T_i = T_c\left[1 + \frac{\mu-1}{b(\mu+1)}\right] \tag{15}$$

Applying the values obtained from eq 12 to eq 15, we obtain T_i = 530 K experimentally, T_i = 971 K (T_c = 615 K, μ = 0.2519, b = −1.028) for the SPC/Ew water model using the KB method, and T_i = 960 K (T_c = 614 K, μ = 0.2533, b = −1.058) using the 2PT method.

3.g. Depth Profile of Surface Energies and the Definition of the Interface. A novel aspect of the 2PT-IFT approach is that it relies solely on atomic velocities from short trajectories, which makes it possible to evaluate the contributions of each molecule to the total free energy, entropy, and enthalpy. This allows us to obtain depth profiles of the thermodynamics. We focus here on the TIP4P/2005 water model since it is particularly good at describing the excess surface enthalpy and entropy, although we show a similar analysis for the other three water models in Supporting Information Figure S5. Analysis of the free energy profile (Figure 5c) reveals long-range tails (slow convergence) and fluctuations that are hidden in the density profile assuming a planar interface (Figure 5a). This free energy profile is a natural consequence of the smooth, monotonically increasing entropy (Figure 5b) and enthalpy (Figure 5d) profiles.

To better examine the interfacial thermodynamics, we assigned the water molecules to particular shells (obtained from the valley−valley distances in the free energy profile) and find that, at 298 K, molecules in the surface layer have on average 11 J/(mol/K) more entropy than the bulk (a 16% increase) but are destabilized by 25 kJ/mol enthalpically. The net result is a 20 kJ/mol decrease in stability compared to the bulk. If we assume a closest packed arrangement of spherical molecules on the surface, each with a radius of 1.9 Å and a molecular surface area of 46.6 Å^2, this means that the surface molecules contribute 71.3 dyn/cm to the surface tension, which is 6−7 dyn/cm greater than the 64.4 dyn/cm total for this water model. This discrepancy can be explained if we consider the thermodynamics of the second layer water molecules, defined as molecules 5−7 Å from the surface. We find that they also have an increase entropy of +2.5 J/(mol/K) compared to the bulk, However, and unlike the surface molecules, they are able to interact with two surrounding water layers and so have a similar enthalpy to the bulk. The net result is that these water molecules are ∼−0.9 kcal/mol more stable than the bulk and so *decrease* the surface tension by 3−4 dyn/cm. A similar analysis on the third layer shows that this layer further decreases the surface tension by 1−2 dyn/cm.

The smooth, monotonically increasing entropy profile for water at the (superhydrophobic) air−water interface stands in contrast to the fluctuating entropy profile calculated for water solvating a hydrophilic DNA molecule,[17] although in both cases, the subsurface water molecules possess more entropy than the bulk. Therefore, we find that although the thermodynamics of interfacial water are complex, there are characteristic signatures that vary in predictable ways. In the case of the air−water interface, the signature is of an entropically stabilized subsurface layer resulting in a free energy minimum in this region (Figure 5c). The free energy minima is consistent with a purported second maximum in the density profile at the subsurface area, obtained from calculations assuming a nonplanar, instantaneous interface.[79]

The slow convergence and nonmonotonicity of the free energy profile also suggests that the exact meaning of the "interface" should be revisited. In the standard definition based on Gibbs theory, the interface is the [90,10] density region: the region between 10% and 90% of the bulk density. This corresponds to 2.17δ, where the interfacial parameter δ is obtained from eq 5 (Supporting Information Table S1) or an interfacial width of 3.44 Å for the TIP4P/2005 water model (Table 4). An alternative definition can be made based on a suggestion by Tolman in his most excellent work on the Gibbs theory of surface tension in 1948.[27] Tolman pointed out that for a liquid−vapor system at equilibrium, the total Gibbs free energy, G, can be conveniently partitioned into three components:

$$G^{\text{total}} = G^{\text{A}} + G^{\text{B}} + G^{\text{I}} \tag{16}$$

Table 4. Calculated Slab Thicknesses and Interfacial Widths of Liquids Considered in This Study[a]

				interfacial width (Å)	
type	liquid	Δz (Å)[b]	δ (Å)	ρ	ΔG
water	TIP4P/2005	43.93	1.57	3.44	7.05
	mW	42.40	1.33	2.93	7.01
	SPC/Ew	43.96	1.62	3.55	7.08
	TIP3P	41.98	1.69	3.70	7.13
polar aprotic	acetonitrile	54.12	4.05	8.90	9.80
	DMSO	40.77	1.67	3.68	4.40
polar protic	hexanol	42.18	2.46	5.41	5.40
	NMA	39.16	1.65	3.62	5.30
apolar	cyclohexane	47.31	3.30	7.25	5.10
	toluene	45.16	2.73	6.01	5.00

[a]The interfacial width calculated from fitting the density profile in (eq 6) and from the free energy profiles are presented. [b]Δz = slab thickness.

dx.doi.org/10.1021/jp410861h | J. Phys. Chem. B 2014, 118, 5943−5956

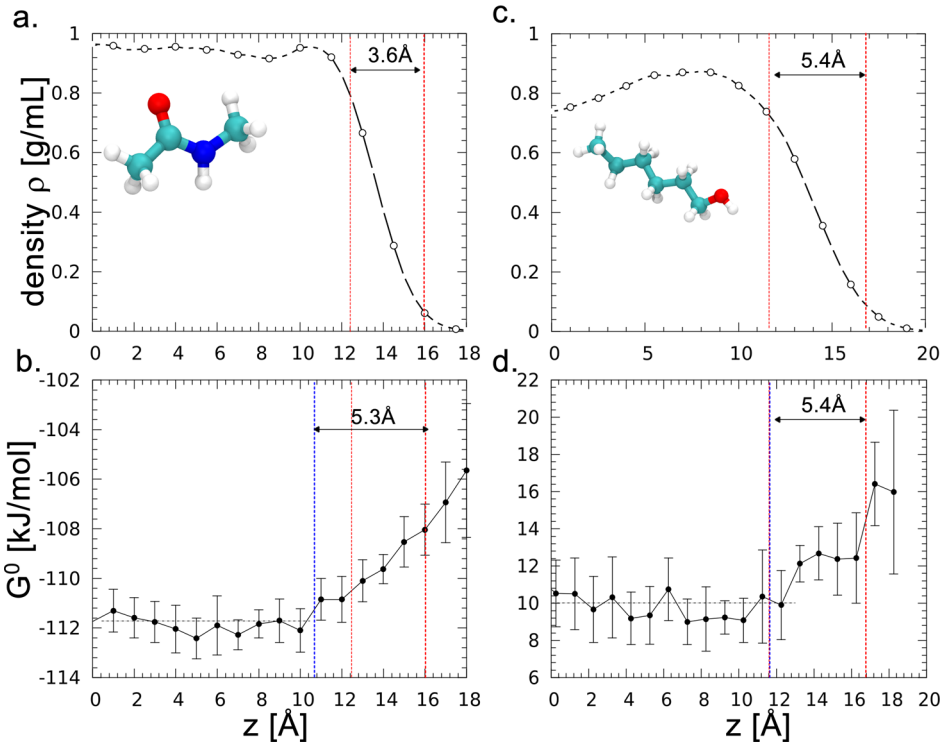

Figure 6. Properties of polar protic liquids. (a) Center of mass (COM) density profile of a slab of 256 NMA molecules described using the OPLS-AA/L force field at 298 K. The density defined interfacial thickness is indicated by the vertical dashed red lines. Inset: Ball and stick representation of NMA. (b) Gibbs free energy profile of NMA calculated using the 2PT method. The bulk liquid free energy is indicated by the dashed horizontal black line. The free energy defined interfacial thickness is indicated as the difference between the dashed blue and dashed red vertical lines. (c) COM density profile of 160 hexanol molecules. (d) Gibbs free energy profile of hexanol calculated using the 2PT method.

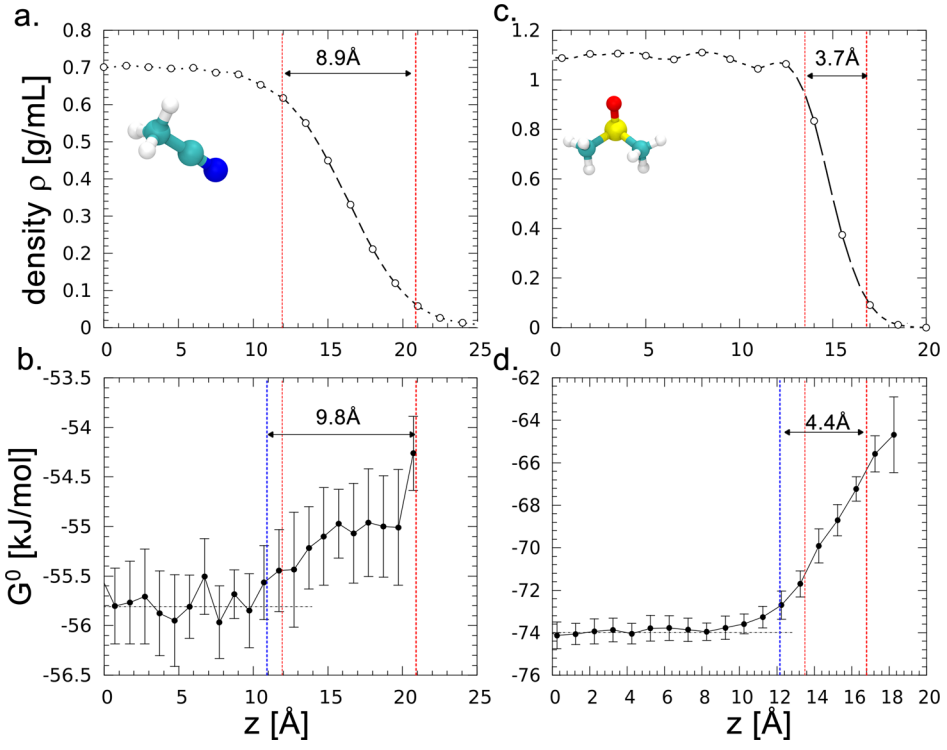

Figure 7. Properties of polar aprotic liquids. (a) COM density profile of a slab of 512 acetonitrile molecules described using the OPLS-AA/L force field at 298 K. (b) Gibbs free energy profile of acetonitrile calculated using the 2PT method. (c) COM density profile of 320 DMSO molecules. (d) Gibbs free energy profile of DMSO.

where G^A and G^B are the free energies of the liquid and vapor phases, and G^I is the free energy of the interface, as defined by the Gibbs dividing surface: a plane of demarcation where the mass and energy flux of each phase is equal and opposite. Inherent in

dx.doi.org/10.1021/jp410861h | J. Phys. Chem. B 2014, 118, 5943−5956

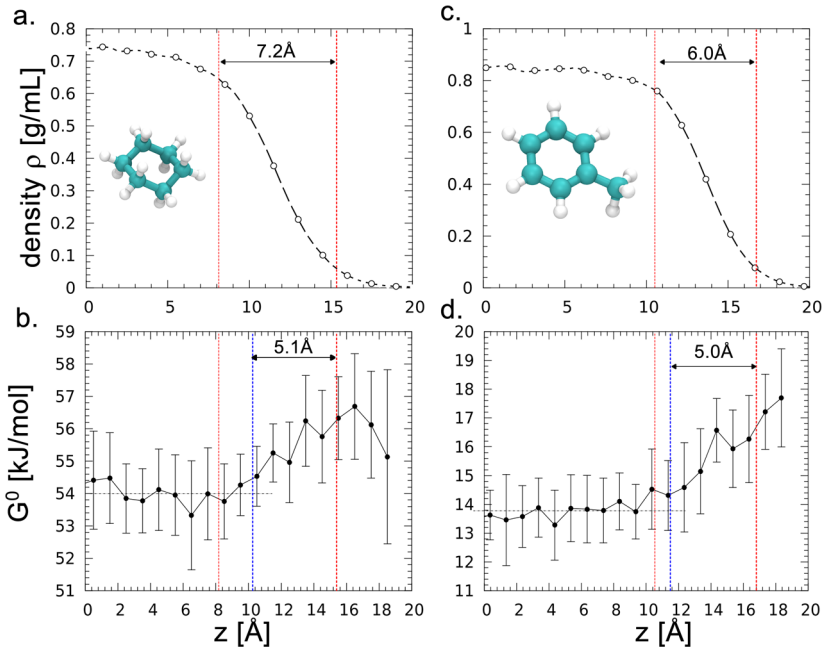

Figure 8. Properties of apolar liquids. (a) COM density profile of a slab of 180 cyclohexane molecules described using the OPLS-AA/L force field at 298 K. (b) Gibbs free energy profile of cyclohexane calculated using the 2PT method. (c) COM density profile of 200 toluene molecules. (d) Gibbs free energy profile of toluene calculated using the 2PT method.

the Tolman definition in eq 16 is the assumption that the interfacial properties of the system are somehow different from that of either component A or B. This leads naturally to a definition of the interface as the region beyond which the thermodynamics converge to the bulk. In the case of the TIP4P/2005 water model, this would result in an interfacial width of 7.1 Å (4.5δ), or twice the interfacial width calculated from the density profile.

3.f. Depth Profiles of Thermodynamics of the Other Liquids. We now consider the trends in the thermodynamic profiles of the six other liquids, but in less detail than for water. For the polar protic liquids, we find that the free energy decreases monotonically (becomes more positive or less stable) toward the surface (Figure 6). Again, we find that the free energy profile converges slower than the density: the interfacial width based on the free energy is 5.3 Å for NMA, compared to 3.6 Å based on the density profile (Table 4). In the case of hexanol, we calculate a free energy interfacial width of 5.4 Å, which is the same as the interfacial width based on the density profile. It appears that this highly extended, nonspherical molecule invalidates the center of mass distributions that we use to determine the average position of the molecules, obscures the molecular structuring and may explain why the density profile in Figure 6c does not appear converged. Finally, in contrast to our results for water, the free energy profiles of both these polar molecules does not show any minimum near the subsurface region.

The pattern of slower convergence of the free energy than for the density also appears to hold for the polar aprotic acetonitrile and DMSO liquids (Figure 7). Here we calculate interfacial widths that increase by 12% and 19% compared to those predicted from the density. On the other hand, for the apolar cyclohexane and toluene liquids we find that the free energy profiles converge faster than the density profile (Figure 8). Decreased ordering at the interface of nonpolar liquids apparently leads to faster convergence.

4. CONCLUSION AND OUTLOOK

We have examined the thermodynamic factors that contribute to the surface tension of pure water between 240 and 375 K by explicit calculations of the surface free energy using the 2PT method. Overall, we find excellent agreement with the standard Kirkwood−Buff scheme based on anisotropy in the stress, but the 2PT-based approach leads to additional insights. For one, we have shown that explicit treatment of the electrostatics is critical for describing the liquid structure at the surface. An attempt to incorporate the electrostatics into two- and three-body van der Waals terms (the mW water model) results in a poor description of the excess surface enthalpies and entropies. We emphasize that the particularly good agreement to the experimental IFT (excess surface free energy) at room temperature of the mW water molecule obscures the fact that the surface thermodynamics and structure are incorrectly predicted. This suggests that the excess surface entropy and enthalpy, and not the IFT, should be used as fitting parameters when developing these water molecules.

Secondly, by analyzing the free energy profile, we find fluctuations that extend far into what would be considered bulk from standard Gibbs theory in the case of polar liquids, leading to interfacial widths that are twice as large as would be expected. Specifically, in the case of water, entropy−enthalpy compensation results in a free energy minima for the subsurface layer. This entropically stabilized layer decreases the surface tension, a potentially important consideration when considering the chemistry at fuel cell electrodes and H_2O oxidation catalysts. Our results could also have important consequences for the location and stability of interfacial ions and small molecules. For example, there have been reports that the surface tension of water actually increases at low enough concentrations of ionic salts.[94,95] One could imagine that these salts perturb the entropic and enthalpic character of the subsurface layer nonuniformly, which could lead to anomalous thermodynamics as a function of salt concentration.

dx.doi.org/10.1021/jp410861h | J. Phys. Chem. B 2014, 118, 5943−5956

■ ASSOCIATED CONTENT

Supporting Information

Table S1 for fitting parameters for fitting the liquid density profile, Figures S1−S4 showing the convergence of the potential energy and IFT with vdW cutoff, the correlation between the IFT of the 2PT and KB methods, and profiles of the thermodynamics of the SPC/Ew, TIP3P, and mW water models, and Figure S5 showing profiles of thermodynamic parameters $G°$, $H°$, and $S°$. This material is available free of charge via the Internet at http://pubs.acs.org.

■ AUTHOR INFORMATION

Corresponding Authors

*(T.A.P.) E-mail: tod.a.cp@gmail.com.
*(W.A.G.) E-mail: wag@wag.caltech.edu.

Present Address

[†]The Molecular Foundry, Lawrence Berkeley National Laboratory, 1 Cyclotron Rd., Berkeley, CA 94720, USA.

Notes

The authors declare no competing financial interest.

■ ACKNOWLEDGMENTS

This work was supported by funds from Dow Chemical Corp. (Willie Lau and Joe Rokowski), National Science Foundation (NSF, Grant CBET-1067848, George Antos), and by the World Class University Program (Grant R31-2008-000-10055-0) and the Integrated Water Technology (IWT) Project (2012M1A2A2026588) funded by the Ministry of Education, Science and Technology through the National Research Foundation of Korea. We are grateful for the support from the Energy, Environment, Water, and Sustainability (EEWS) Initiative funding from the Korea Advanced Institute of Science and Technology (KAIST).

■ REFERENCES

(1) Kiss, G.; Tombacz, E.; Hansson, H. C. Surface Tension Effects of Humic-Like Substances in the Aqueous Extract of Tropospheric Fine Aerosol. *J. Atmos. Chem.* **2005**, *50*, 279−294.

(2) De Gennes, P. G.; Taupin, C. Microemulsions and the Flexibility of Oil/Water Interfaces. *J. Phys. Chem.* **1982**, *86*, 2294−2304.

(3) Wilson, K. R.; Cavalleri, M.; Rude, B. S.; Schaller, R. D.; Nilsson, A.; Pettersson, L. G. M.; Goldman, N.; Catalano, T.; Bozek, J. D.; Saykally, R. J. Characterization of Hydrogen Bond Acceptor Molecules at the Water Surface Using Near-Edge X-Ray Absorption Fine-Structure Spectroscopy and Density Functional Theory. *J. Phys.: Condens. Matter* **2002**, *14*, L221−L226.

(4) Kuo, I. F. W.; Mundy, C. J. An Ab Initio Molecular Dynamics Study of the Aqueous Liquid-Vapor Interface. *Science* **2004**, *303*, 658−660.

(5) Kühne, T. D.; Pascal, T. A.; Kaxiras, E.; Jung, Y. New Insights into the Structure of the Vapor/Water Interface from Large-Scale First-Principles Simulations. *J. Phys. Chem. Lett.* **2011**, *2*, 105−113.

(6) Du, Q.; Superfine, R.; Freysz, E.; Shen, Y. R. Vibrational Spectroscopy of Water at the Vapor Water Interface. *Phys. Rev. Lett.* **1993**, *70*, 2313−2316.

(7) Cappa, C. D.; Smith, J. D.; Wilson, K. R.; Saykally, R. J. Revisiting the Total Ion Yield X-Ray Absorption Spectra of Liquid Water Microjets. *J. Phys.: Condens. Matter* **2008**, *20*, 205105−205112.

(8) Kathmann, S. M.; Kuo, I. F. W.; Mundy, C. J.; Schenter, G. K. Understanding the Surface Potential of Water. *J. Phys. Chem. B* **2011**, *115*, 4369−4377.

(9) Wick, C. D.; Kuo, I. F. W.; Mundy, C. J.; Dang, L. X. The Effect of Polarizability for Understanding the Molecular Structure of Aqueous Interfaces. *J. Chem. Theory Comput.* **2007**, *3*, 2002−2010.

(10) Kathmann, S. M.; Kuo, I. F. W.; Mundy, C. J. Electronic Effects on the Surface Potential at the Vapor−Liquid Interface of Water. *J. Am. Chem. Soc.* **2008**, *130*, 16556−16561.

(11) Baer, M. D.; Stern, A. C.; Levin, Y.; Tobias, D. J.; Mundy, C. J. Electrochemical Surface Potential Due to Classical Point Charge Models Drives Anion Adsorption to the Air−Water Interface. *J. Phys. Chem. Lett.* **2012**, *3*, 1565−1570.

(12) Mishra, H.; Enami, S.; Nielsen, R. J.; Hoffmann, M. R.; Goddard, W. A.; Colussi, A. J. Anions Dramatically Enhance Proton Transfer through Aqueous Interfaces. *Proc. Natl. Acad. Sci. U. S. A.* **2012**, DOI: 10.1073/pnas.1200949109.

(13) Pascal, T. A.; Scharf, D.; Jung, Y.; Kuhne, T. D. On the Absolute Thermodynamics of Water from Computer Simulations: A Comparison of First-Principles Molecular Dynamics, Reactive and Empirical Force Fields. *J. Chem. Phys.* **2012**, *137*, No. 244507.

(14) Pascal, T. A.; Lin, S. T.; Goddard, W. A., III. Thermodynamics of Liquids: Standard Molar Entropies and Heat Capacities of Common Solvents from 2 pt Molecular Dynamics. *Phys. Chem. Chem. Phys.* **2011**, *13*, 169−181.

(15) Pascal, T. A.; Lin, S.-T.; Goddard, W.; Jung, Y. Stability of Positively Charged Solutes in Water: A Transition from Hydrophobic to Hydrophilic. *J. Phys. Chem. Lett.* **2012**, *3*, 294−298.

(16) Lee, S. G.; Pascal, T. A.; Koh, W.; Brunello, G. F.; Goddard, W. A.; Jang, S. S. Deswelling Mechanisms of Surface-Grafted Poly(Nipaam) Brush: Molecular Dynamics Simulation Approach. *J. Phys. Chem. C* **2012**, *116*, 15974−15985.

(17) Pascal, T. A.; Goddard, W. A.; Maiti, P. K.; Vaidehi, N. Role of Specific Cations and Water Entropy on the Stability of Branched DNA Motif Structures. *J. Phys. Chem. B* **2012**, *116*, 12159−12167.

(18) Pascal, T. A.; Goddard, W. A. Hydrophobic Segregation, Phase Transitions and the Anomalous Thermodynamics of Water/Methanol Mixtures. *J. Phys. Chem. B* **2012**, *116*, 13905−13912.

(19) Pascal, T. A.; He, Y.; Jiang, S.; Goddard, W. A. Thermodynamics of Water Stabilization of Carboxybetaine Hydrogels from Molecular Dynamics Simulations. *J. Phys. Chem. Lett.* **2011**, *2*, 1757−1760.

(20) We will use the terms internal energy and enthalpy interchangeably from now on, noting that the terms differ slightly by a change in density term (δV) of the interfacial region.

(21) Binder, K. Monte Carlo Calculation of the Surface Tension for Two- and Three-Dimensional Lattice-Gas Models. *Phys. Rev. A* **1982**, *25*, 1699−1709.

(22) Vega, C.; de Miguel, E. Surface Tension of the Most Popular Models of Water by Using the Test-Area Simulation Method. *J. Chem. Phys.* **2007**, *126*, 154707−154710.

(23) Ghoufi, A.; Malfreyt, P. Calculation of the Surface Tension and Pressure Components from a Non-Exponential Perturbation Method of the Thermodynamic Route. *J. Chem. Phys.* **2012**, *136*, 024104−024106.

(24) Gloor, G. J.; Jackson, G.; Blas, F. J.; de Miguel, E. Test-Area Simulation Method for the Direct Determination of the Interfacial Tension of Systems with Continuous or Discontinuous Potentials. *J. Chem. Phys.* **2005**, *123*, 134703−134719.

(25) de Miguel, E.; Jackson, G. The Nature of the Calculation of the Pressure in Molecular Simulations of Continuous Models from Volume Perturbations. *J. Chem. Phys.* **2006**, *125*, 164109−164111.

(26) Ismail, A. E.; Grest, G. S.; Stevens, M. J. Capillary Waves at the Liquid-Vapor Interface and the Surface Tension of Water. *J. Chem. Phys.* **2006**, *125*, -.

(27) Tolman, R. C. Consideration of the Gibbs Theory of Surface Tension. *J. Chem. Phys.* **1948**, *16*, 758−774.

(28) Kirkwood, J. G.; Buff, F. P. The Statistical Mechanical Theory of Surface Tension. *J. Chem. Phys.* **1949**, *17*, 338−343.

(29) Jang, S. S.; Lin, S. T.; Maiti, P. K.; Blanco, M.; Goddard, W. A.; Shuler, P.; Tang, Y. C. Molecular Dynamics Study of a Surfactant-Mediated Decane−Water Interface: Effect of Molecular Architecture of Alkyl Benzene Sulfonate. *J. Phys. Chem. B* **2004**, *108*, 12130−12140.

(30) Rivera, J. L.; Predota, M.; Chialvo, A. A.; Cummings, P. T. Vapor−Liquid Equilibrium Simulations of the Scpdp Model of Water. *Chem. Phys. Lett.* **2002**, *357*, 189−194.

(31) Alejandre, J.; Tildesley, D. J.; Chapela, G. A. Molecular Dynamics Simulation of the Orthobaric Densities and Surface Tension of Water. *J. Chem. Phys.* **1995**, *102*, 4574−4583.
(32) Huang, D. M.; Geissler, P. L.; Chandler, D. Scaling of Hydrophobic Solvation Free Energies. *J. Phys. Chem. B* **2001**, *105*, 6704−6709.
(33) Feller, S. E.; Pastor, R. W.; Rojnuckarin, A.; Bogusz, S.; Brooks, B. R. Effect of Electrostatic Force Truncation on Interfacial and Transport Properties of Water. *J. Phys. Chem.* **1996**, *100*, 17011−17020.
(34) Shi, B.; Sinha, S.; Dhir, V. K. Molecular Dynamics Simulation of the Density and Surface Tension of Water by Particle-Particle Particle-Mesh Method. *J. Chem. Phys.* **2006**, *124*, 204715−204717.
(35) Taylor, R. S.; Dang, L. X.; Garrett, B. C. Molecular Dynamics Simulations of the Liquid/Vapor Interface of Spc/E Water. *J. Phys. Chem.* **1996**, *100*, 11720−11725.
(36) Zakharov, V. V.; Brodskaya, E. N.; Laaksonen, A. Surface Properties of Water Clusters: A Molecular Dynamics Study. *Mol. Phys.* **1998**, *95*, 203−209.
(37) Dang, L. X.; Chang, T.-M. Molecular Dynamics Study of Water Clusters, Liquid, and Liquid–Vapor Interface of Water with Many-Body Potentials. *J. Chem. Phys.* **1997**, *106*, 8149−8159.
(38) Sokhan, V. P.; Tildesley, D. J. The Free Surface of Water: Molecular Orientation, Surface Potential and Nonlinear Susceptibility. *Mol. Phys.* **1997**, *92*, 625−640.
(39) Chen, F.; Smith, P. E. Simulated Surface Tensions of Common Water Models. *J. Chem. Phys.* **2007**, *126*, 221101−221103.
(40) Wynveen, A.; Bresme, F. Interactions of Polarizable Media in Water: A Molecular Dynamics Approach. *J. Chem. Phys.* **2006**, *124*, 104502−104508.
(41) Drost-Hansen, W. Aqueous Interfaces—Methods of Study and Structural Properties. Part Two. *Ind. Eng. Chem.* **1965**, *57*, 18−37.
(42) Lin, S. T.; Blanco, M.; Goddard, W. A. The Two-Phase Model for Calculating Thermodynamic Properties of Liquids from Molecular Dynamics: Validation for the Phase Diagram of Lennard-Jones Fluids. *J. Chem. Phys.* **2003**, *119*, 11792−11805.
(43) Lin, S. T.; Maiti, P. K.; Goddard, W. A. Two-Phase Thermodynamic Model for Efficient and Accurate Absolute Entropy of Water from Molecular Dynamics Simulations. *J. Phys. Chem. B* **2010**, *114*, 8191−8198.
(44) Berendsen, H. J. C.; Grigera, J. R.; Straatsma, T. P. The Missing Term in Effective Pair Potentials. *J. Phys. Chem.* **1987**, *91*, 6269−6271.
(45) Abascal, J.; Vega, C. A General Purpose Model for the Condensed Phases of Water: Tip4p/2005. *J. Chem. Phys.* **2005**, *123*, 234505.
(46) McQuarrie, D. A. *Statistical Mechanics*; University Science Books: Sausalito, CA, USA, 2000.
(47) Allen, M. P.; Tildesley, D. J. *Computer Simulation of Liquids*; Clarendon Press, Oxford University Press: Oxford [England], New York, 1987.
(48) Carnahan, N. F.; Starling, K. E. Thermodynamic Properties of a Rigid-Sphere Fluid. *J. Chem. Phys.* **1970**, *53*, 600−603.
(49) Desjarlais, M. P. First-Principles Calculation of Entropy for Liquid Metals. *Phys. Rev. E* **2013**, *88*, 062145.
(50) Eyring, H.; Ree, T. Significant Liquid Structures, VI. The Vacancy Theory of Liquids. *Proc. Natl. Acad. Sci. U. S. A.* **1961**, *47*, 526−537.
(51) Huang, S.-N.; Pascal, T. A.; Goddard, W. A.; Maiti, P. K.; Lin, S.-T. Absolute Entropy and Energy of Carbon Dioxide Using the Two-Phase Thermodynamic Model. *J. Chem. Theory Comput.* **2011**, *7*, 1893−1901.
(52) Zhang, C.; Spanu, L.; Galli, G. Entropy of Liquid Water from ab Initio Molecular Dynamics. *J. Phys. Chem. B* **2011**, *115*, 14190−14195.
(53) Gross, A. S.; Bell, A. T.; Chu, J.-W. Entropy of Cellulose Dissolution in Water and in the Ionic Liquid 1-Butyl-3-Methylimidazolim Chloride. *Phys. Chem. Chem. Phys.* **2012**, *14*, 8425−8430.
(54) GhattyVenkataKrishna, P. K.; Alekozai, E. M.; Beckham, G. T.; Schulz, R.; Crowley, M. F.; Uberbacher, E. C.; Cheng, X. Initial Recognition of a Cellodextrin Chain in the Cellulose-Binding Tunnel May Affect Cellobiohydrolase Directional Specificity. *Biophys. J.* **2013**, *104*, 904−912.
(55) Tian, J.; Sethi, A.; Swanson, B. I.; Goldstein, B.; Gnanakaran, S. Taste of Sugar at the Membrane: Thermodynamics and Kinetics of the Interaction of a Disaccharide with Lipid Bilayers. *Biophys. J.* **2013**, *104*, 622−632.
(56) Wallace, A. F.; Hedges, L. O.; Fernandez-Martinez, A.; Raiteri, P.; Gale, J. D.; Waychunas, G. A.; Whitelam, S.; Banfield, J. F.; De Yoreo, J. J. Microscopic Evidence for Liquid-Liquid Separation in Supersaturated Caco3 Solutions. *Science* **2013**, *341*, 885−889.
(57) Huber, R. G.; Fuchs, J. E.; von Grafenstein, S.; Laner, M.; Wallnoefer, H. G.; Abdelkader, N.; Kroemer, R.; Liedl, K. R. Entropy from State Probabilities: Hydration Entropy of Cations. *J. Phys. Chem. B* **2013**, *117*, 6466−6472.
(58) Kemmer, F. N. *Water, the Universal Solvent*; Nalco Chemical Co.: Oak Brook, IL, USA, 1977.
(59) Boates, B.; Bonev, S. A. Demixing Instability in Dense Molten MgSiO_{3} and the Phase Diagram of MgO. *Phys. Rev. Lett.* **2013**, *110*, 135504.
(60) Teweldeberhan, A.; Boates, B.; Bonev, S. Co_2 in the Mantle: Melting and Solid−Solid Phase Boundaries. *Earth Planet. Sci. Lett.* **2013**, *373*, 228−232.
(61) Jorgensen, W. L.; Chandrasekhar, J.; Madura, J. D.; Impey, R. W.; Klein, M. L. Comparison of Simple Potential Functions for Simulating Liquid Water. *J. Chem. Phys.* **1983**, *79*, 926−935.
(62) Molinero, V.; Moore, E. B. Water Modeled as an Intermediate Element between Carbon and Silicon. *J. Phys. Chem. B* **2008**, *113*, 4008−4016.
(63) Jorgensen, W. L.; Tiradorives, J. The OPLS [Optimized Potentials for Liquid Simulations] Potential Functions for Proteins, Energy Minimizations for Crystals of Cyclic-Peptides and Crambin. *J. Am. Chem. Soc.* **1988**, *110*, 1657−1666.
(64) Kaminski, G. A.; Friesner, R. A.; Tirado-Rives, J.; Jorgensen, W. L. Evaluation and Reparametrization of the OPLS-AA Force Field for Proteins via Comparison with Accurate Quantum Chemical Calculations on Peptides. *J. Phys. Chem. B* **2001**, *105*, 6474−6487.
(65) Plimpton, S. Fast Parallel Algorithms for Short-Range Molecular-Dynamics. *J. Comput. Phys.* **1995**, *117*, 1−19.
(66) Ryckaert, J. P.; Ciccotti, G.; Berendsen, H. J. C. Numerical-Integration of Cartesian Equations of Motion of a System with Constraints—Molecular-Dynamics of N-Alkanes. *J. Comput. Phys.* **1977**, *23*, 327−341.
(67) Maiti, P. K.; Çağın, T.; Wang, G.; Goddard, W. A. Structure of Pamam Dendrimers: Generations 1 through 11. *Macromolecules* **2004**, *37*, 6236−6254.
(68) Cagin, T.; Wang, G. F.; Martin, R.; Breen, N.; Goddard, W. A. Molecular Modelling of Dendrimers for Nanoscale Applications. *Nanotechnology* **2000**, *11*, 77−84.
(69) Hockney, R. W.; Eastwood, J. W. *Computer Simulation Using Particles*; Taylor & Francis: New York, 1989.
(70) Shinoda, W.; Shiga, M.; Mikami, M. Rapid Estimation of Elastic Constants by Molecular Dynamics Simulation under Constant Stress. *Phys. Rev. B* **2004**, *69*, No. 134103.
(71) Martyna, G. J.; Tobias, D. J.; Klein, M. L. Constant-Pressure Molecular-Dynamics Algorithms. *J. Chem. Phys.* **1994**, *101*, 4177−4189.
(72) Parrinello, M.; Rahman, A. Polymorphic Transitions in Single-Crystals—A New Molecular-Dynamics Method. *J. Appl. Phys.* **1981**, *52*, 7182−7190.
(73) Tuckerman, M. E.; Alejandre, J.; Lopez-Rendon, R.; Jochim, A. L.; Martyna, G. J. A Liouville-Operator Derived. Measure-Preserving Integrator for Molecular Dynamics Simulations in the Isothermal-Isobaric Ensemble. *J. Phys. A: Math. Gen.* **2006**, *39*, 5629−5651.
(74) Yeh, I. C.; Berkowitz, M. L. Ewald Summation for Systems with Slab Geometry. *J. Chem. Phys.* **1999**, *111*, 3155−3162.
(75) Bresme, F.; Chacon, E.; Tarazona, P. Molecular Dynamics Investigation of the Intrinsic Structure of Water-Fluid Interfaces Via the Intrinsic Sampling Method. *Phys. Chem. Chem. Phys.* **2008**, *10*, 4704−4715.
(76) Chacón, E.; Tarazona, P.; Alejandre, J. The Intrinsic Structure of the Water Surface. *J. Chem. Phys.* **2006**, *125*, -.
(77) Tarazona, P.; Chacón, E.; Reinaldo-Falagán, M.; Velasco, E. Layering Structures at Free Liquid Surfaces: The Fisher−Widom Line and the Capillary Waves. *J. Chem. Phys.* **2002**, *117*, 3941−3950.

(78) Chacón, E.; Reinaldo-Falagán, M.; Velasco, E.; Tarazona, P. Layering at Free Liquid Surfaces. *Phys. Rev. Lett.* **2001**, *87*, 166101.
(79) Willard, A. P.; Chandler, D. Instantaneous Liquid Interfaces. *J. Phys. Chem. B* **2010**, *114*, 1954−1958.
(80) Alejandre, J.; Chapela, G. A. The Surface Tension of Tip4p/2005 Water Model Using the Ewald Sums for the Dispersion Interactions. *J. Chem. Phys.* **2010**, *132*, 014701−014706.
(81) Friedel, J. Metallic Alloys. *Nuovo Cimento* **1958**, *7* (Suppl. 2), 287−311.
(82) Lide, D. R. *CRC Handbook of Chemistry and Physics*; CRC Press: Boca Raton, FL, USA and London, 1993.
(83) Baron, R.; Molinero, V. Water-Driven Cavity−Ligand Binding: Comparison of Thermodynamic Signatures from Coarse-Grained and Atomic-Level Simulations. *J. Chem. Theory Comput.* **2012**, *8*, 3696−3704.
(84) *NIST Chemistry Webbook*, Reference Database No. 69; National Institute of Standards and Technology: Gaithersburg, MD, USA, 2000.
(85) Wagner, W.; Pruss, A. The IAPWS Formulation 1995 for the Thermodynamic Properties of Ordinary Water Substance for General and Scientific Use. *J. Phys. Chem. Ref. Data* **2002**, *31*, 387−535.
(86) Vargaftik, N. B.; Volkov, B. N.; Voljak, L. D. International Tables of the Surface-Tension of Water. *J. Phys. Chem. Ref. Data* **1983**, *12*, 817−820.
(87) Rivera, J. L.; Starr, F. W.; Paricaud, P.; Cummings, P. T. Polarizable Contributions to the Surface Tension of Liquid Water. *J. Chem. Phys.* **2006**, *125*, -.
(88) Caleman, C.; van Maaren, P. J.; Hong, M.; Hub, J. S.; Costa, L. T.; van der Spoel, D. Force Field Benchmark of Organic Liquids: Density, Enthalpy of Vaporization, Heat Capacities, Surface Tension, Isothermal Compressibility, Volumetric Expansion Coefficient, and Dielectric Constant. *J. Chem. Theory Comput.* **2011**, *8*, 61−74.
(89) National Research Council, Washburn E. W. West C. J. Hull C. *International Critical Tables of Numerical Data, Physics, Chemistry and Technology*; Published for the National Research Council by the McGraw-Hill: New York, 1926.
(90) Gittens, G. J. Variation of Surface Tension of Water with Temperature. *J. Colloid Interface Sci.* **1969**, *30*, 406−412.
(91) Cini, R.; Loglio, G.; Ficalbi, A. Temperature Dependence of Surface-Tension of Water by Equilibrium Ring Method. *J. Colloid Interface Sci.* **1972**, *41*, 287−297.
(92) Jasper, J. J. The Surface Tension of Pure Liquid Compounds. *J. Phys. Chem. Ref. Data* **1972**, *1*, 841−1010.
(93) Johansson, K.; Eriksson, J. C. Determination of $D\gamma/Dt$ for Water by Means of a Differential Technique. *J. Colloid Interface Sci.* **1972**, *40*, 398−405.
(94) Jones, G.; Ray, W. A. The Surface Tension of Solutions of Electrolytes as a Function of the Concentration. I. A Differential Method for Measuring Relative Surface Tension. *J. Am. Chem. Soc.* **1937**, *59*, 187−198.
(95) Petersen, P. B.; Johnson, J. C.; Knutsen, K. P.; Saykally, R. J. Direct Experimental Validation of the Jones−Ray Effect. *Chem. Phys. Lett.* **2004**, *397*, 46−50.
(96) Kroenlein, K.; Muzny, C.; Kazakov, A.; Diky, V.; Chirico, R.; Magee, J.; Abdulagatov, I.; Frenkel, M. *NIST/TRC Web Thermo Tables (WTT)*; Technical Report Version 2-2011-4-Pro; National Institute of Standards and Technology: Gaithersburg, MD, USA, 2011; http://wtt-pro.nist.gov/wtt-pro, accessed Mar. 21, 2014.